

Article

The Gaseous Hydrogen Transport Capacity in Nanopores Coupling Bulk Flow Mechanisms and Surface Diffusion: Integration of Profession and Innovation

Yanglu Wan ¹, Wei Lu ¹, Zhouman Huang ¹, Rucang Qian ¹ and Zheng Sun ^{1,2,*}

¹ School of Innovation and Entrepreneurship, Wuchang University of Technology, Wuhan 430200, China; wanyanglu870225@gmail.com (Y.W.); 120160587@wut.edu.cn (W.L.); zmhuang0826@126.com (Z.H.); a18751258443@hotmail.com (R.Q.)

² State Key Laboratory for Fine Exploration and Intelligent Development of Coal Resources, China University of Mining and Technology, Xuzhou 221116, China

* Correspondence: sunzheng@cumt.edu.cn

Abstract: Due to its unique chemical structure, hydrogen energy inherently has a high calorific value without reinforcing global warming, so it is expected to be a promising alternative energy source in the future. In this work, we focus on nanoconfined hydrogen flow performance, a critical issue in terms of geological hydrogen storage. For nanopores where the pore scale is comparable to hydrogen's molecular size, the impact on hydrogen molecules exerted by the pore surface cannot be neglected, leading to the molecules near the surface gaining mobility and slipping on the surface. Furthermore, hydrogen adsorption takes place in the nanopores, and the way the adsorption molecules move is completely different from the bulk molecules. Hence, the frequently applied Navier–Stokes equation, based on the no-slip boundary condition and overlooking the contribution of the adsorption molecules, fails to precisely predict the hydrogen flow capacity in nanopores. In this paper, hydrogen molecules are classified as bulk molecules and adsorption molecules, and then models for the bulk hydrogen and the adsorption hydrogen are developed separately. In detail, the bulk hydrogen model considers the slip boundary and rarefaction effect characterized by the Knudsen number, while the flow of the adsorption hydrogen is driven by a chemical potential gradient, which is a function of pressure and the essential adsorption capacity. Subsequently, a general model for the hydrogen flow in nanopores is established through weight superposition of the bulk hydrogen flow as well as the adsorption hydrogen, and the key weight coefficients are determined according to the volume proportion of the identified area. The results indicate that (a) the surface diffusion of the adsorption molecules dominates the hydrogen flow capacity inside nanopores with a pore size of less than 5 nm; (b) improving the pressure benefits the bulk hydrogen flow and plays a detrimental role in reducing surface diffusion at a relatively large pressure range; (c) the nanoconfined hydrogen flow conductance with a strong adsorption capacity ($P_L = 2$ MPa) could reach a value ten times greater than that with a weak adsorption capacity ($P_L = 10$ MPa). This research provides a profound framework for exploring hydrogen flow behavior in ultra-tight strata related to adsorption phenomena.

Keywords: hydrogen; flow capacity; nanopores; adsorption; surface diffusion



Citation: Wan, Y.; Lu, W.; Huang, Z.; Qian, R.; Sun, Z. The Gaseous Hydrogen Transport Capacity in Nanopores Coupling Bulk Flow Mechanisms and Surface Diffusion: Integration of Profession and Innovation. *Processes* **2024**, *12*, 972. <https://doi.org/10.3390/pr12050972>

Academic Editor: Michael C. Georgiadis

Received: 1 April 2024

Revised: 30 April 2024

Accepted: 9 May 2024

Published: 10 May 2024



Copyright: © 2024 by the authors. Licensee MDPI, Basel, Switzerland. This article is an open access article distributed under the terms and conditions of the Creative Commons Attribution (CC BY) license (<https://creativecommons.org/licenses/by/4.0/>).

1. Introduction

With the current purpose of reducing CO₂ emissions and mitigating the greenhouse effect, intensifying the utilization of clean energy [1,2], like solar energy, wind energy and hydrogen energy, is urgent. In particular, hydrogen energy is well recognized as a promising energy source for the future, as its use is totally free of CO₂ emissions [3,4]. As reported, geological hydrogen storage is a practical approach to promoting the development of the hydrogen industry, and accurately evaluating the hydrogen flow behavior inside favorable

geological sites is crucial, yet relevant methods are lacking [5]. Meanwhile, in light of the adsorption mechanisms enabling considerably large hydrogen storage, geological sites rich in nanopores favor efficient hydrogen storage [6,7]. Currently, classic no-slip hydrodynamics theory, like the Navier–Stokes equation or the Darcy function, is mainly utilized to evaluate hydrogen flow capacity at the macroscopic scale. And the Knudsen diffusion equation is always utilized to describe hydrogen flow at the nanoscale [8,9], inherently considering hydrogen flow’s physics. However, in terms of geological hydrogen storage with a wide range of pressure and temperatures, hydrogen flow physics could involve a continuum flow, slip flow or transition flow as well as Knudsen diffusion. Thus, characterizing a nanoconfined hydrogen flow using solely the Knudsen diffusion equation inevitably leads to erroneous predictions. Essentially, hydrogen flow under nanoconfinement behaves completely different from a conventional flow [10,11]. As a result, hydrogen transport behavior through nanopores is an evident knowledge gap, important to field applications of geological hydrogen storage. This research intends to shed light on the hydrogen flow capacity in nanopores, a key aspect of hydrogen storage in ultra-tight strata.

Both the hydrogen storage mode and flow mechanism are responsible for a varying hydrogen flow capacity compared to that understood according to the classic hydrodynamics theory. Regarding the storage mode, the hydrogen molecules inside nanopores are clearly divided into two types, encompassing adsorption molecules and bulk molecules [12]. In comparison, there are only bulk hydrogen molecules in large-scale pores. Strong surface–molecule interactions result in the presence of adsorption molecules, which are a function of the surface–molecule distance and can be neglected in large pores, widely confirmed by molecular simulation and experimental observations [13,14]. Regarding the flow mechanism, lots of experimental evidence on the basis of advanced microfluid devices demonstrates that molecules at the nanopore wall can move at a certain velocity, the so-called slip phenomenon, quantified by the slip length, directly conflicting with the fundamental no-slip boundary condition of the aforementioned classic theory [15,16]. Other than that, it is believed that adsorption molecules can move by hopping from a low-energy spot to another, showing its dramatic difference from bulk hydrogen [17]. After clarifying the original reasons leading to the unusual hydrogen flow in nanopores, it is necessary to establish a model for the hydrogen flow in nanopores instead of utilizing traditional no-slip methods. In recent years, research dedicated to nanoconfined gas flow has mainly focused on methane, CO₂ and vapor water instead of hydrogen [18,19]. Typically, Beskok and Karniadakis investigated the gas flow in smooth channels and modified the traditional Navier–Stokes equation by incorporating the second-order boundary condition [20]. The modified equation had a good match with the simulation results and experimental data. Additionally, the impact of pore geometry on gas flow capacity was investigated [21,22]. Unfortunately, models accounting for the slip boundary condition fail to capture the contribution of adsorption gas. After further investigation, there exist four gas flow regimes, including continuum flow, slip flow, transition flow and Knudsen diffusion [23,24], which can be classified using the Knudsen number. Tremendous research effort has been dedicated to developing a unified gas flow model that can be applied to the entire Knudsen number range or, in other words, that can represent these four different flow regimes. Shi et al. displayed the difference in the flow capacity of different flow regimes and established a general gas flow model through weight superposition of the continuum flow and Knudsen flow [25]. Notably, the weight coefficients proposed have no physical meaning, and the validity of the general model is still in doubt. Wu et al. demonstrated the inherent physics leading to the varying flow regimes’ varying Knudsen numbers is the relative strength between intermolecular collisions and molecule–wall collisions [26]. After that, the weight coefficients were derived based on the collision probability, and a fully covered model was proposed according to weight superposition of the slip flow and Knudsen diffusion. In particular, the proposed model could directly degenerate to slip flow at a low Knudsen number and Knudsen diffusion at a high Knudsen number, embodying its rationality from a theoretical viewpoint. Other than focusing on the development of a gas

flow model, the impacts of residual water, multiple components and effective pore size shrinkage due to stress dependence have been investigated in detail in recent years [27,28]. The high-pressure physical properties of hydrogen are different from methane, resulting in the summarized flow behavior of methane not being applicable to nanoconfined hydrogen. Accordingly, little research has been conducted on hydrogen flow in nanopores, and related methods for evaluating hydrogen flow in geological storage are extremely lacking. Exploring hydrogen flow behavior in nanopores is urgent. In this paper, the model for hydrogen flow in nanopores accounts for not only the bulk hydrogen flow mechanism but also the way adsorption molecules move, so-called surface diffusion. Separately, models for bulk hydrogen and adsorption hydrogen are established. Adsorption molecules would occupy a certain area near the nanopore wall; as a result, the area where bulk hydrogen flows shrinks and is actually less than the original total pore area. The weight coefficients for surface diffusion and bulk gas flow are determined according to the volume proportion of the area for adsorption hydrogen and the area excluding the adsorption area, respectively. After that, a general model for nanoconfined hydrogen flow is established according to weight superposition of the bulk gas flow and the surface diffusion of the adsorption hydrogen. After figuring out the hydrogen flow behavior at the nanopore scale, porous modeling using numerical simulation [29] or multiscale modeling [30] accounting for the nanoconfined hydrogen flow could characterize the hydrogen flow behavior at the core scale, which could have direct practical implications for geological hydrogen storage.

The research content is arranged as follows. The physical model displaying the nanoconfined hydrogen flow physics, including the slip boundary for bulk hydrogen and the surface diffusion for adsorption hydrogen, is provided first. Then, theoretical models for the bulk hydrogen flow and surface diffusion are introduced, weight coefficients based on the volume proportion are derived and a general model for hydrogen flow in nanopores is developed. After that, the relationships between nanoconfined hydrogen flow behavior and pressure, temperature and adsorption capacity are revealed. Ultimately, several conclusions are drawn.

2. Physical Model

Gas flow physics varies a lot across scales, resulting in large discrepancies in flow capacity, which could correspond to several magnitudes of discrepancy, as reported [31]. As illustrated in Figure 1, adsorption molecules at the macroscopic scale can be neglected, and the bulk hydrogen at the pore wall is stationary, the so-called no-slip boundary condition. Also, the molecular velocity distribution across the macroscopic pore follows a parabolic curve [32,33]. In comparison, hydrogen molecules tend to accumulate near the microscopic wall as a result of the strong attraction force due to the pore wall, and an adsorption phenomenon occurs. The molecules in the middle of the nanopore further from the pore wall behave exactly like bulk hydrogen. Thus, there are two molecular types (bulk hydrogen and adsorption hydrogen) inside nanopores. The unique feature to which attention should be paid is that the bulk hydrogen near the wall gains mobility and can move at a certain velocity, improving the overall transport efficiency for nanoconfined hydrogen. In addition, the adsorption molecules hop from a low-energy spot to another along the micropore wall after activation, mainly driven by the chemical potential gradient. The way adsorption molecules move is called surface diffusion, a totally new flow physics that conventional models at the macroscale fail to consider. Meanwhile, it is necessary to elaborate the magnitude of the difference between microscopic flow and macroscopic flow. Inherently, gas flow physics can be classified into four types according to the Knudsen number (Kn), with its definition as the mean free path to the characteristic length (see Equation (2)), including continuum flow ($Kn \leq 10^{-3}$), slip flow ($10^{-3} \leq Kn < 10^{-2}$), transition flow ($10^{-2} \leq Kn < 10$) and Knudsen diffusion ($Kn > 10$). Since the slip phenomenon and the surface diffusion by the adsorption molecules have an insignificant role in affecting the total flow capacity when the gas flow physics corresponds to continuum flow, the difference in the flow capacity across different scales is fairly small and can be neglected. With an

increasing Kn , the contributions from slip and the adsorption molecules become more and more evident, and the difference cannot be overlooked. As a result, the magnitude of the difference heavily depends on whether Kn exceeds 10^{-3} or not, so newly emerging flow mechanisms like slip and surface diffusion should be considered when Kn is greater than 10^{-3} ; otherwise, the classic Navier–Stokes equation still holds.

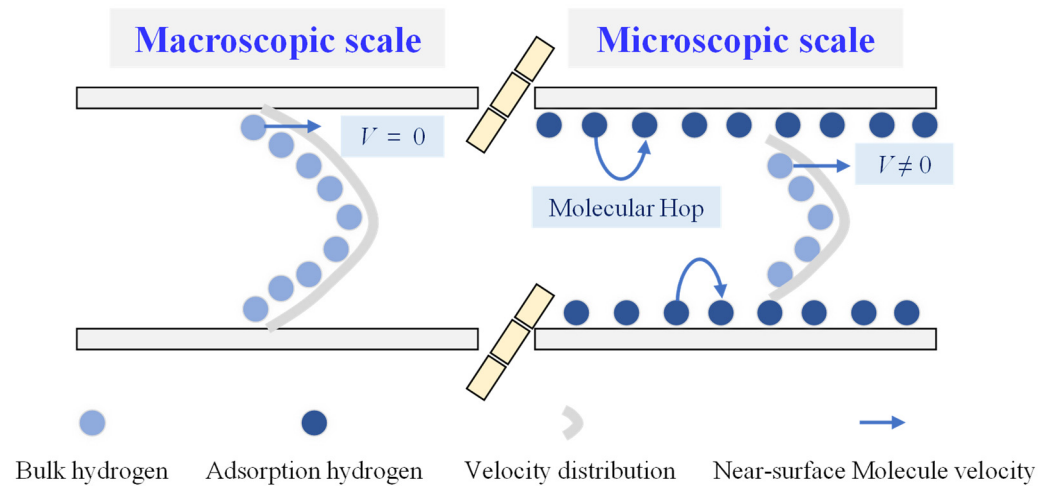


Figure 1. Hydrogen flow behavior over pore scales.

The essential reasons why traditional models break down when it comes to nanoconfined gas flow are the slip boundary as well as the surface diffusion contributed by the adsorption molecules. Motivated by the hydrogen flow physics at the nanoscale, research should incorporate the slip boundary conditions and the surface diffusion mechanism into a modified bulk gas flow model. Also, key environmental parameters, including pressure and temperature, affecting the physical properties of the bulk hydrogen and the relative volume proportion of the adsorption hydrogen, are fully coupled in the developed model. The interactions between the adsorption molecules and bulk molecules are characterized according to monolayer adsorption theory.

3. Model Establishment

The essential model framework for nanoconfined hydrogen flow is weight superposition of the bulk hydrogen flow and adsorption hydrogen surface diffusion. Models for bulk hydrogen and surface diffusion will be provided below, respectively.

3.1. Nanoconfined Bulk Hydrogen Flow Mechanism

Several boundary conditions have been proposed to capture the gas slip phenomenon [34,35], and it has been demonstrated that a no-slip equation incorporating the second-order boundary condition permits an excellent fit for the gas flow performance through a flat nanopore wall. The basic formula for gas slip flow is as follows.

$$J_{bulk} = \frac{r^2 p M}{8 \mu R T} (1 + \alpha Kn) \left(1 + \frac{4 Kn}{1 - b Kn} \right) \frac{dp}{dl} \quad (1)$$

where J_{bulk} is the mass flux of the bulk hydrogen flow, $\text{Kg}/\text{m}^2/\text{s}$; r is the nanopore radius, nm ; p is the hydrogen pressure, MPa ; M is hydrogen's molar weight, 2 g/mol ; μ is hydrogen's viscosity, cp ; R is the gas's universal constant, 8.314 J/mol/K ; T is the temperature, K ; α represents the rarefaction effect, indicating increasing molecule–wall collisions, dimensionless; b is a constant related to the applied boundary condition, which is -1 for the second-order boundary condition; l is the distance in the hydrogen flow direction, m ; Kn is

the Knudsen number, defined as the ratio of the mean free path to the nanopore size [36], dimensionless.

$$Kn = \frac{\lambda}{2r} \quad (2)$$

$$\lambda = \frac{\mu}{p} \sqrt{\frac{\pi RT}{2M}} \quad (3)$$

where λ is the mean free path of hydrogen, indicating the distance a bulk hydrogen molecule can move between two adjacent collision accidents, m.

Considering the second-order boundary condition and the weight coefficient of the bulk gas flow, hydrogen's mass conductance is contributed to by the bulk flow mechanism.

$$J_{bulk} = \zeta_{bulk} \frac{r^2 p M}{8\mu RT} (1 + \alpha Kn) \left(1 + \frac{4Kn}{1 + Kn}\right) \frac{dp}{dl} \quad (4)$$

$$\alpha = \alpha_o \frac{2}{\pi} \tan^{-1}(\alpha_1 Kn^\beta) \quad (5)$$

where ζ_{bulk} is the weight coefficient for the bulk gas flow, defined as the ratio of the cross-section area where the bulk gas flows to the entire nanopore cross-section area, dimensionless; α_o , α_1 and β are constants to represent the rarefaction effect, dimensionless.

$$C_{bulk} = \zeta_{bulk} \frac{r^2 p M}{8\mu RT} (1 + \alpha Kn) \left(1 + \frac{4Kn}{1 + Kn}\right) \quad (6)$$

where C_{bulk} is the hydrogen flow conductance derived from Equation (4), manifesting hydrogen's mass conductance per the pressure gradient, s.

Hydrogen's viscosity is described as a function of pressure and temperature [37,38]; the formulas below can give satisfactory predictions that have been well validated using experimental data.

$$P_r = P/P_c \quad (7)$$

$$T_r = T/T_c \quad (8)$$

$$\mu = \mu_o \left[1 + \frac{A_1}{T_r^5} \left(\frac{P_r^4}{T_r^{20} + P_r^4} \right) + A_2 \left(\frac{P_r}{T_r} \right)^2 + A_3 \left(\frac{P_r}{T_r} \right) \right] \quad (9)$$

where P_c and T_c are the critical pressure and critical temperature, respectively; P_r and T_r are reduced pressure and reduced temperature, respectively; μ_o is hydrogen's viscosity under standard conditions, which is 0.0087 cp.

3.2. Surface Diffusion of Adsorption Hydrogen

Unlike the bulk hydrogen flow driven by a pressure gradient, the chemical potential gradient is the main force promoting the surface diffusion of the adsorption hydrogen. In accordance with the fundamental surface chemistry, the chemical potential is a function of the gas concentration [39], and the following expression is utilized to evaluate the concentration of adsorption hydrogen.

$$C_{sc} = \frac{4\theta M}{\pi d_m^3 N_A} \quad (10)$$

where C_{sc} is the adsorption hydrogen concentration, Kg/m³; N_A is the Avogadro constant; d_m is the hydrogen molecular size, 0.23 nm; θ is the cover ratio, indicating the ratio of occupied spots to the entire available spots on the nanopore wall, which has the following expression, dimensionless.

$$\theta = \frac{p}{p + p_L} \quad (11)$$

where P_L is the Langmuir pressure constant for monolayer adsorption theory, and a smaller P_L indicates a stronger adsorption capacity, MPa.

In accordance with the Maxwell–Stefan method, as molecular mobility due to surface diffusion is much less than that due to adsorption–desorption, the gas conductance promoted by surface diffusion is as follows:

$$J_{surface} = D_s \frac{C_{sc}}{p} \frac{dp}{dl} \quad (12)$$

where D_s is the surface diffusion coefficient, m^2/s .

The surface diffusion coefficient is correlated with the hydrogen cover ratio described by Equation (11), and the surface diffusion coefficient at a cover ratio (D_s^0) of zero has the following expression.

$$D_s^0 = 8.29 \times 10^{-7} T^{0.5} \exp\left(-\frac{\Delta H^{0.8}}{RT}\right) \quad (13)$$

where ΔH is the isothermal adsorption heat for each instant of hydrogen adsorption activity, J/mol.

The surface diffusion coefficient at a specified cover ratio can be described as a function of the surface diffusion coefficient at a cover ratio of zero and the given cover ratio, as presented below.

$$D_s = D_s^0 \frac{(1 - \theta) + \frac{\kappa}{2}\theta(2 - \theta) + \{H(1 - \kappa)\}(1 - \kappa)\frac{\kappa}{2}\theta^2}{(1 - \theta + \frac{\kappa}{2}\theta)^2} \quad (14)$$

Furthermore, accounting for the weight coefficient of the adsorption hydrogen, the mass conductance as a result of surface diffusion is as follows.

$$J_{surface} = \zeta_{surf} D_s \frac{C_{sc}}{p} \frac{dp}{dl} \quad (15)$$

And the conductance from the surface diffusion is derived below.

$$C_{surface} = \zeta_{surf} D_s \frac{C_{sc}}{p} \quad (16)$$

where $C_{surface}$ is the conductance contributed by surface diffusion, s.

3.3. Model for Hydrogen Transport Capacity

As clarified in Figure 1, the nanoconfined hydrogen flow consists of the bulk hydrogen flow and the surface diffusion of the adsorption hydrogen. Models for both the bulk gas flow and surface diffusion are established, respectively, in this section, while weight coefficients are derived for weight superposition of the bulk gas flow and the surface diffusion. In essence, the weight coefficients are obtained according to the volume proportions of the bulk gas and adsorption hydrogen. As illustrated in Figure 2, assuming uniformly distributed adsorption hydrogen in the nanopores [40,41], the thickness of the adsorption hydrogen in the cross-section at a certain pressure and temperature is uniform as well, described by the following formula.

$$r_d = r_H \frac{p}{p + p_L} \quad (17)$$

where r_d is the thickness of the adsorption hydrogen, nm; r_H is hydrogen's molecular size, 0.23 nm.

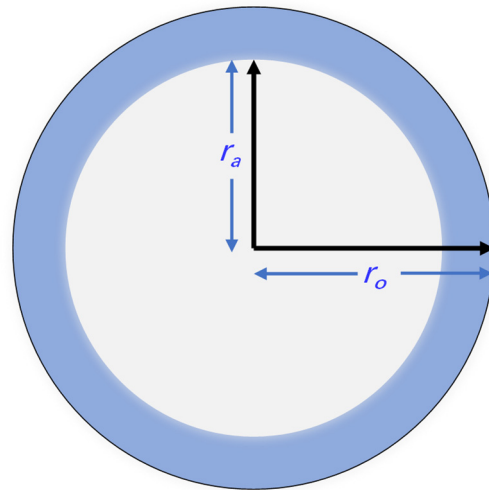


Figure 2. Original nanopore size containing adsorption hydrogen thickness.

In accordance with Equation (17), the thickness of the adsorption hydrogen is equal to hydrogen's molecular size, fitting well with the monolayer precondition, and the thickness would be increasingly reduced with a decline in pressure.

Excluding the area that the adsorption hydrogen molecules occupy, the size of the area for the bulk hydrogen flow is as follows.

$$r_a = r_o - r_d \quad (18)$$

where r_o is the original nanopore size, nm.

The volume proportion for the bulk gas flow is the ratio of the bulk flow area to the whole cross-section, which has the following expression.

$$\zeta_{bulk} = \frac{(r_o - r_d)^2}{r_o^2} \quad (19)$$

$$\zeta_{surf} = 1 - \frac{(r_o - r_d)^2}{r_o^2} \quad (20)$$

Based on the weight coefficients and the effective pore size for the bulk hydrogen flow, the total conductance for hydrogen flow through nanopores is as follows.

$$C_t = \zeta_{bulk} \frac{r_a^2 p M}{8 \mu R T} (1 + \alpha K n) \left(1 + \frac{4 K n}{1 + K n}\right) + \zeta_{surf} D_s \frac{C_{sc}}{p} \quad (21)$$

To evaluate the nanoconfined hydrogen flow capacity in accordance with the proposed model, the thickness of adsorption hydrogen should be obtained using Equation (17) first. Then, the effective pore size for the bulk gas flow and the hydrogen flow conductance contributed by the bulk gas flow using the effective pore size can be calculated using Equation (18) and Equation (6), respectively. After that, the hydrogen conductance contributed by surface diffusion is evaluated using Equations (10)–(16). Finally, the total gas conductance can be obtained through weight superposition of the bulk gas flow and surface diffusion based on Equation (21).

In order to verify the reliability of Equation (21), two sets of experimental data collected from Zamirian et al. are utilized here [42], which accurately examined the apparent permeability of N_2 and CO_2 flowing through different ultra-tight cores. The basic parameters for the experiments are provided in Table 1. The pore size falls into the nanoscale, and the experiments inherently consider a shrinkage in pore size due to the presence of the adsorption phase, as well as surface diffusion. The experimental data are able to clarify the

validity of the proposed model. To facilitate comparison, the apparent permeability and the diffusion coefficient further derived from Equation (21) are given below.

$$K_t = \zeta_{bulk} \frac{r_a^2}{8\mu} (1 + \alpha Kn) \left(1 + \frac{4Kn}{1 + Kn}\right) + \zeta_{surf} D_s \frac{RT C_{sc}}{p^2 M} \quad (22)$$

$$D_t = \zeta_{bulk} \frac{r_a^2 p}{8\mu} (1 + \alpha Kn) \left(1 + \frac{4Kn}{1 + Kn}\right) + \zeta_{surf} D_s \frac{C_{sc} RT}{p M} \quad (23)$$

where K_t is the apparent gas permeability, mD; D_t is the apparent diffusion coefficient, m^2/s .

Table 1. Parameters used to examine the model reliability.

Gas Type	Pore Size	Temperature, K	Pressure, MPa	Possibility for Molecular Blockage or Migration	Langmuir Pressure, MPa
N ₂	3.2 nm	300 K	0.5~3.5 MPa	0.5	4 MPa
CO ₂	5.6 nm	300 K	0.5~2.7 MPa	0.5	1.7 MPa
Helium-3	10.0 nm	40~400 K	~0 MPa	/	/

Comparing the apparent permeability predicted using Equation (22) with the experimental data, Figure 3A manifests that the prediction results on the x -axis have a satisfactory match with the experimental data on the y -axis. Upon analysis, the largest deviation between the model predictions and the data on N₂ or CO₂ flow behavior is 12.7%, and the average difference is only 6.3%, which verifies the reliability of the proposed model. Other than that, considering the relatively large difference in the kinetic diameters of hydrogen and N₂ or CO₂, another dataset for Helium-3's flow capacity through nanopores is added [8], which has a similar kinetic diameter to hydrogen. As presented in Figure 3B, the proposed model has a good match with the results on Helium-3's flow; the average error is 4.8%, further highlighting the accuracy of the proposed model. Notably, the proposed model designed for the nanopore scale may lead to errors when applied to predicting gas flow at the core scale, as the pore size distribution, spatial geometric topological structure and coordinate number accentuate its complexity. Also, the gas's real effects, with varying physical properties of the gas, particularly under high-pressure conditions, influence the gas flow capacity, which, however, are not incorporated into the proposed model. In short, the basic framework for evaluating the hydrogen flow capacity in nanopores is well verified, and some modifications could be implemented to improve the model accuracy in the future.

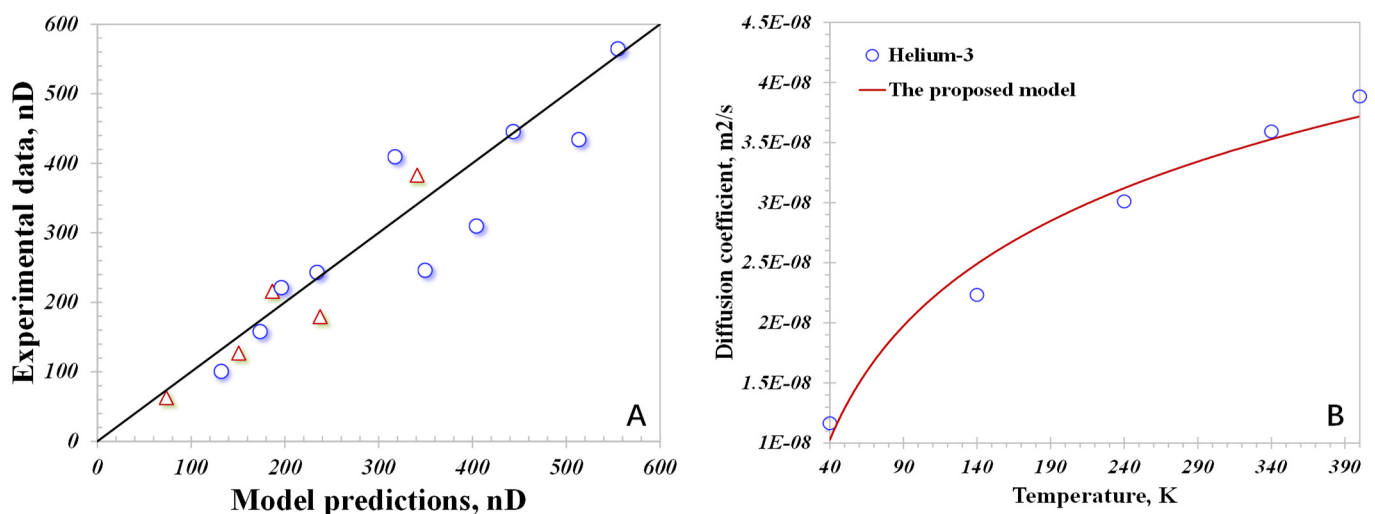


Figure 3. Clarifying the model reliability using different gas types: (A) N₂ and CO₂; (B) Helium-3.

4. Results and Discussion

In terms of geological hydrogen storage inside ultra-tight reservoirs, the influences of pore size, pressure, temperature and adsorption capacity are identified in detail on the basis of the proposed model. In order to avoid the discrepancies caused by uncertainty [43], the basic parameters investigated in this section are listed in Table 2; all the parameter ranges are sourced from the actual field across the world.

Table 2. Parameters to explore nanoconfined hydrogen flow behavior.

Temperature, K	Pressure, MPa	Pore Size, nm	Langmuir Pressure, MPa	Adsorption Heat at Zero Cover Ratio, J/mol	Molar Weight, g/mol
320~460	0~50	2~60	2~10	14,000	2
Possibility of molecular blockage or migration	Universal gas constant, J/mol/k	Molecular size, nm	Critical pressure, MPa	Critical temperature, K	Hydrogen viscosity under standard conditions, cp
0.5	8.314	0.23	1.67	38.2	0.0087

4.1. Nanoscale Pore Size

In this section, temperature and pressure remain unchanged at 400 K and 10 MPa, respectively. The pore size ranges from 1 to 60 nm. As displayed in Figure 4, the blue line representing the total conductance indicates that the total hydrogen flow capacity first declines and then enhances with an increasing pore size. In other words, there exists a key pore size corresponding to the weakest total conductance, which is approximately 11 nm in this case. This phenomenon conflicts with the traditional principle in macro pores that the fluid flow capacity increases with an increasing pore size. In order to evidently show the variation between the total conductance and pore size, the deviation representing the difference between the total conductance at a certain pore size and that at 2 nm is illustrated in red in Figure 4. The total conductance at 2 nm may be 2.5 times greater than that at the weakest flow capacity. When the pore size exceeds 12 nm, the total conductance increases with an increasing pore size, matching well with the above principle. Therefore, this demonstrated that an atypical decline in the total conductance with an increasing pore size takes place inside nanopores of less than 12 nm.

To explore the underlying cause of this atypical decline, the two hydrogen flow mechanisms, the bulk gas flow and surface diffusion, are further investigated. As stated in the establishment of the model, the two mechanisms fully contribute to the total conductance, and their individual contributions are presented in Figure 5. For a pore size of less than 10 nm, the contribution from surface diffusion is evidently greater than that of the bulk hydrogen flow. And the surface diffusion becomes more dominant with a smaller pore size: the contribution of surface diffusion surprisingly reaches 99.1% for 2 nm pores. It worth noting that the contribution from surface diffusion dramatically reduces with an increasing pore size, which declines to 1.5% for 60 nm pores. In pores larger than 30 nm, the surface diffusion actually can be neglected since its contribution is less than 10%, as applied to macroscopic models of hydrogen flow. Therefore, the total conductance for small nanopores (less than 10 nm) is mainly governed by surface diffusion, while that for large nanopores (over 30 nm) is mainly contributed to by the bulk flow mechanism. It is this difference leading to the weakest total conductance at 11 nm presented in Figure 4. When the pore size ranges from 2 to 10 nm, surface diffusion plays a key role in affecting the total hydrogen flow capacity, whose role is reduced with an increasing pore size. On the contrary, when the pore size exceeds 30 nm, the contribution from surface diffusion is negligible, and the total conductance is controlled by the bulk gas flow, whose role is increased with an increasing pore size. As a result, the dominant role of surface diffusion in <10 nm pores is potentially responsible for our atypical observation. Hence, the flow

capacity of small nanopores is always underestimated due to the unique surface diffusion neglected, which actually could be as strong as that of pores larger than 30 nm based on the proposed model predictions. An accurate prediction of the hydrogen flow in nanopores should account for the contribution of small nanopores, particularly those smaller than 10 nm.

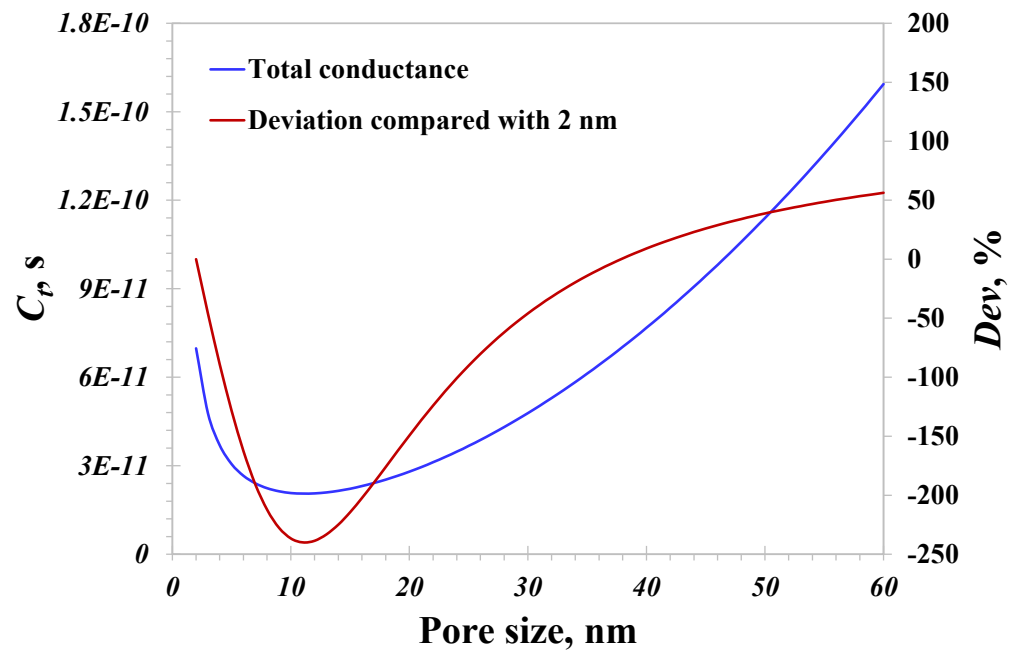


Figure 4. Total hydrogen conductance versus nanopore size.

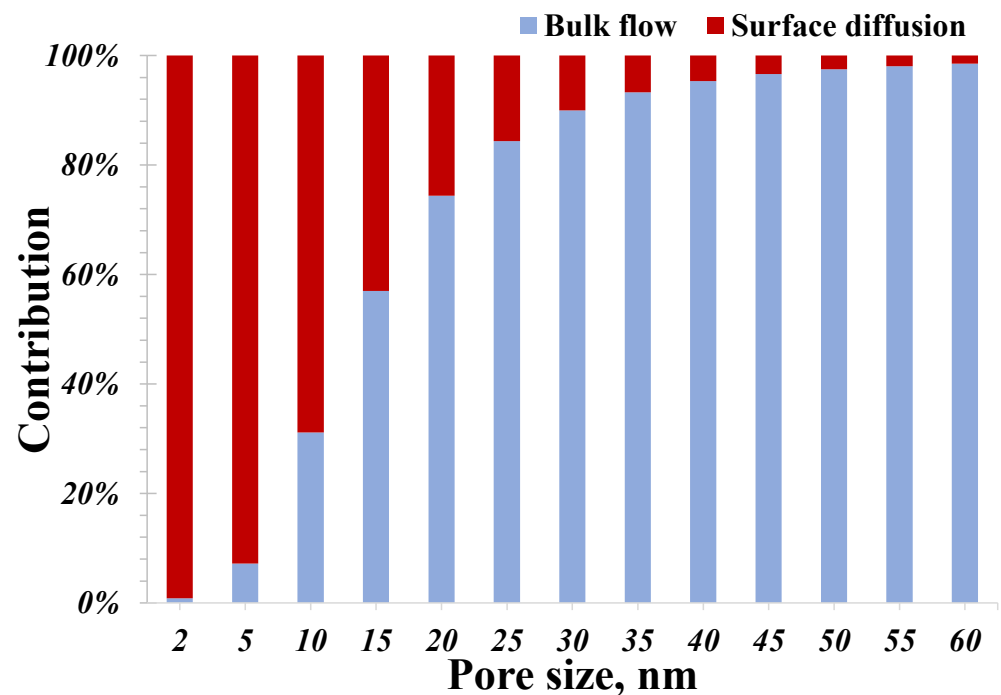


Figure 5. Contributions of nanoconfined hydrogen flow mechanism vary with pore size.

4.2. Temperature and Pressure

Since the temperature and pressure of ultra-tight geological sites suitable for hydrogen storage have wide ranges, their impacts on the nanoconfined hydrogen flow capacity are worth revealing. The pore size in this section remains unchanged at 10 nm. As displayed in

Figure 6, when the temperature is 400 K, the total conductance is rapidly enhanced at first in the 0–10 MPa pressure range, and this increasing gradient declines dramatically at pressures exceeding 20 MPa. In other words, there are typically two different modes of enhancement in the total conductance with increasing pressure, and the magnitude of the increase in the low pressure range (<10 MPa) is much greater than that in high pressure range (>20 MPa) in this case. In general, the total conductance of hydrogen greatly improves with increasing pressure. Basically, a high-pressure environment would mitigate the molecular slip at the boundary, therefore mitigating the total conductance from this viewpoint. On the other hand, increasing pressure favors the greater contribution of the adsorption molecules, as demonstrated by the conductance of the surface diffusion over pressure in Figure 6. More importantly, the bulk flow capacity intensifies, as hydrogen's density has an almost linearly increasing correlation with increasing pressure, also demonstrated in Figure 6. The inherent mechanism behind the rapidly increasing total conductance in the low pressure range is mainly caused by variations in the surface diffusion capacity depending on pressure. Also, it can be observed that surface diffusion plays a more prominent role in low-pressure conditions, and considering the observations in Figure 5, neglecting the contribution from surface diffusion in small nanopores (<10 nm) at a relatively low pressure would lead to an evident underestimation of the total hydrogen conductance.

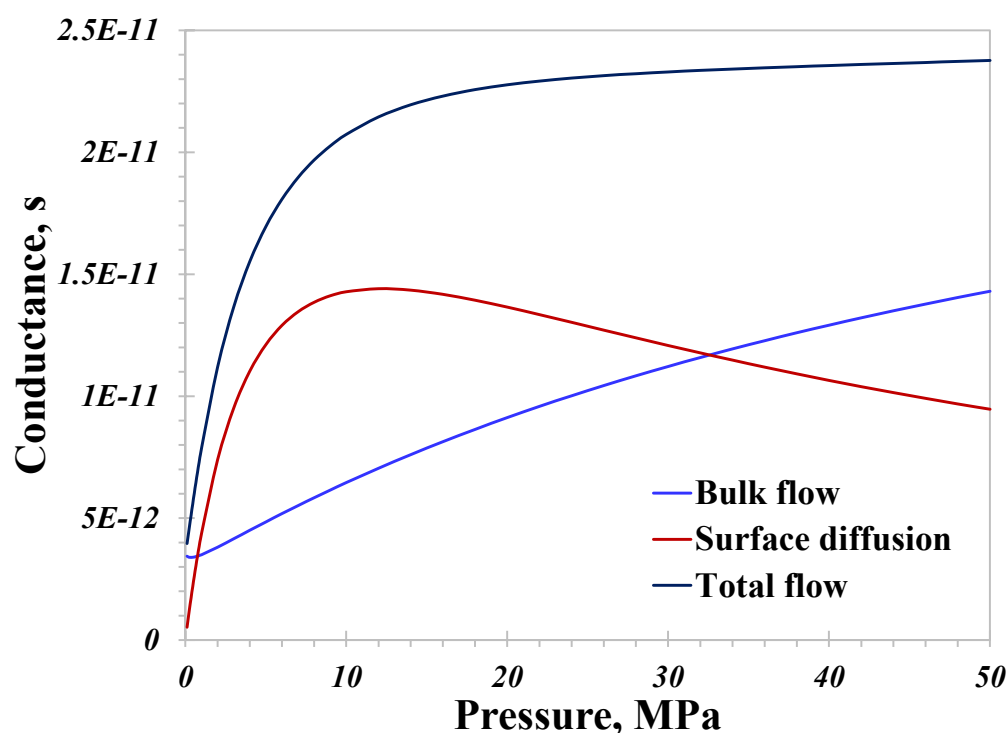


Figure 6. Nanoconfined hydrogen flow conductance versus pressure.

Basically, the relationship between the total hydrogen conductance and pressure is mainly dominated by surface diffusion in small nanopores and by the bulk flow mechanism in large nanopores. As a result, the variation in the total conductance of the hydrogen flow inside nanopores depending on pressure may change at different pore sizes, which is confirmed, as displayed in Figure 7. For 30 nm nanopores, the total conductance is always enhanced with an increasing pressure, and the magnitude of the increase in the low pressure range (<10 MPa) is greater than that in the high pressure range. Inherently, both surface diffusion and the bulk flow benefit the nanoconfined hydrogen flow capacity in the low pressure range; however, surface diffusion gradually has a detrimental effect on mitigating the total conductance in the high pressure range, as presented in Figure 6. In contrast, the total conductance in 3 nm nanopores totally coincides with surface diffusion, which would

increase rapidly at first and then decrease stably with increasing pressure. Therefore, for nanopores with a pore size of less than about 10 nm, there exists a peak total conductance at a certain pressure, which is 9 MPa in this investigation. As for geological hydrogen storage, improving the pressure is an effective approach to reducing the hydrogen flow capacity for ultra-tight storage sites rich in nanopores less than 10 nm in size. On the contrary, if the majority of the nanopores are larger than 30 nm, improving the pressure would dramatically promote the hydrogen flow capacity. Therefore, the pore size distribution of geological sites that are suitable for hydrogen storage is crucial to the hydrogen flow behavior.

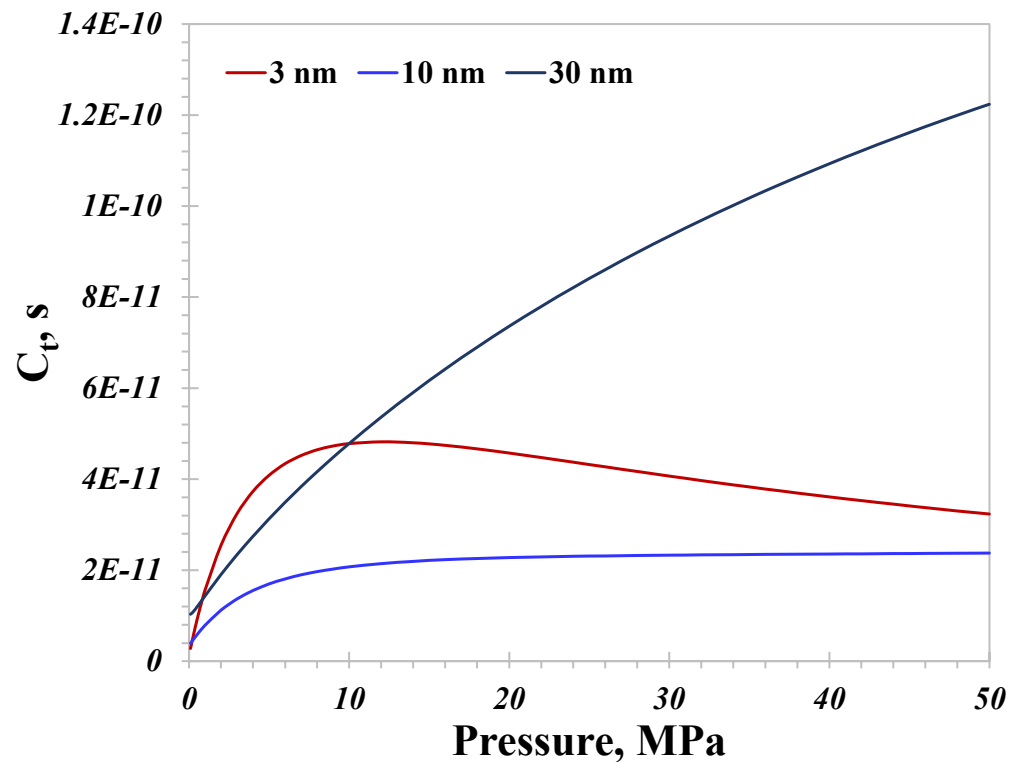


Figure 7. Total hydrogen flow conductance with different pore sizes versus pressure.

Then, temperature ranging from 320 to 450 K is set to examine its effect on the hydrogen flow capacity in nanopores. The pressure and pore size are unchanged at 10 MPa and 10 nm in this case, respectively. As illustrated in Figure 8, the conductance from the bulk flow declines with an increasing temperature, which can be attributed to the following two reasons. On the one hand, a high temperature would supply more free energy to the hydrogen molecules and reinforce intermolecular collisions as well as molecule–wall collisions, promoting the slip phenomenon and improving the bulk flow capacity. On the other hand, hydrogen’s density declines fast with an increasing temperature, reducing the bulk flow capacity. Other than that, the reducing density has a stronger influence on the bulk flow capacity than the increasingly evident slip phenomenon under high-temperature conditions. The conductance contributed by surface diffusion has a linearly increasing correlation with the increase in temperature. Enhancing the temperature benefits the adsorption hydrogen’s activation, which is good for surface diffusion. In this calculation, the total flow conductance increases as the temperature increases. Similarly, in small nanopores (<10 nm) where surface diffusion is prominent in affecting the total conductance, the total conductance increases with an increasing temperature, matching well with the surface diffusion. On the contrary, the total conductance would decline with an increasing temperature in >30 nm nanopores, as the bulk flow mechanism dominates. Therefore, the relationship between temperature and the total hydrogen flow capacity is closely linked to the pore size distribution.

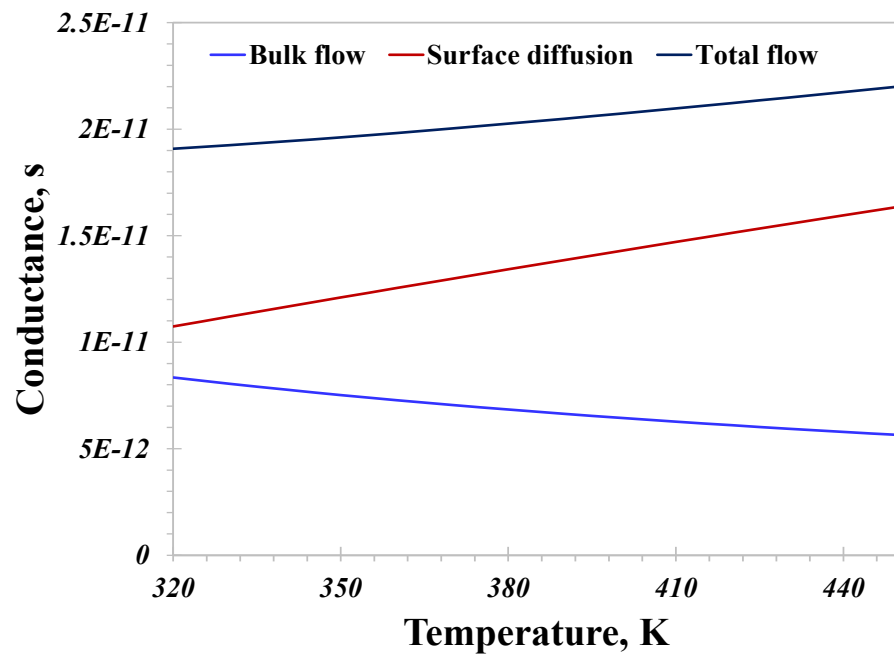


Figure 8. Nanoconfined hydrogen flow conductance versus temperature.

4.3. Adsorption Capacity

From a microscopic viewpoint, the attraction force that nanopore walls impose on hydrogen molecules varies with different surface compositions. Hence, there exists a great discrepancy in the adsorption capacity of different geological sites suitable for hydrogen storage. As depicted in Figure 9, four sets of Langmuir curves are used, and the total hydrogen conductance over the adsorption capacity is investigated. The pore size is set as 5 nm in this calculation.

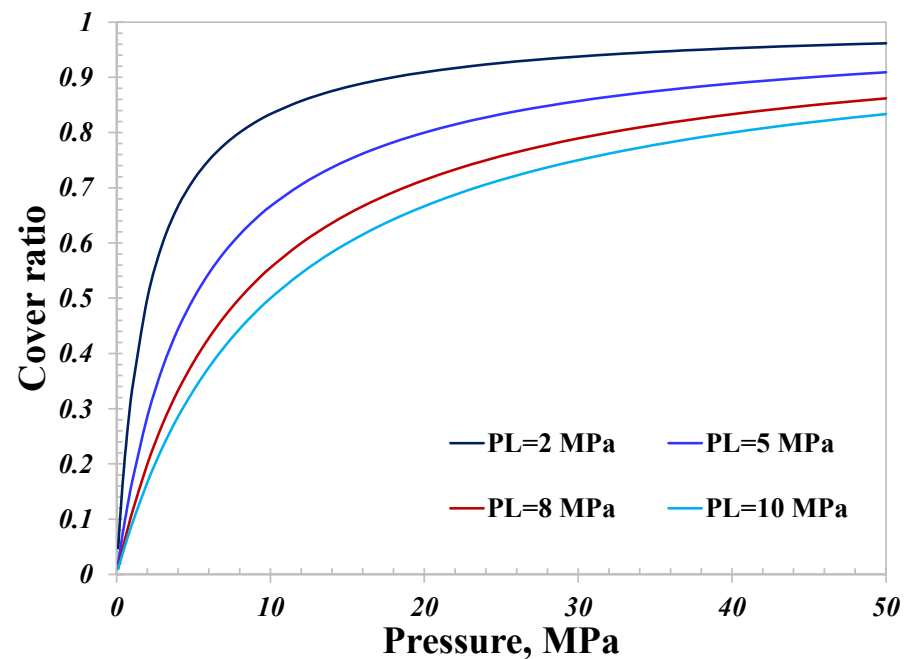


Figure 9. Hydrogen cover ratio versus adsorption capacity represented by P_L .

As illustrated in Figure 10, since surface diffusion dominates when the pore size is 5 nm, the total conductance with different P_L values almost shows the same variation as

surface diffusion. The total conductance with a strong adsorption capacity is much greater than that with a weak adsorption capacity. The peak conductance with P_L equal to 2 MPa is about 10 times that with P_L equal to 10 MPa, as demonstrated in Figure 11, manifesting the significant impact the adsorption capacity can have on the nanoconfined hydrogen capacity. As a result, there would be a stronger hydrogen flow capacity for geological sites with a strong adsorption capacity than those with a weak capacity; the magnitude could reach as surprisingly high as several orders. In light of the variation of the surface diffusion with pressure, increasing the pressure is a practical method to reduce the total conductance. As presented in Figure 11, manipulating the pressure from 6 MPa to 50 MPa could reduce the total conductance when P_L is 2 MPa by over 50%. Considering the investigated impact of temperature on the total conductance, decreasing the temperature could also reduce the total hydrogen conductance for small nanopores.

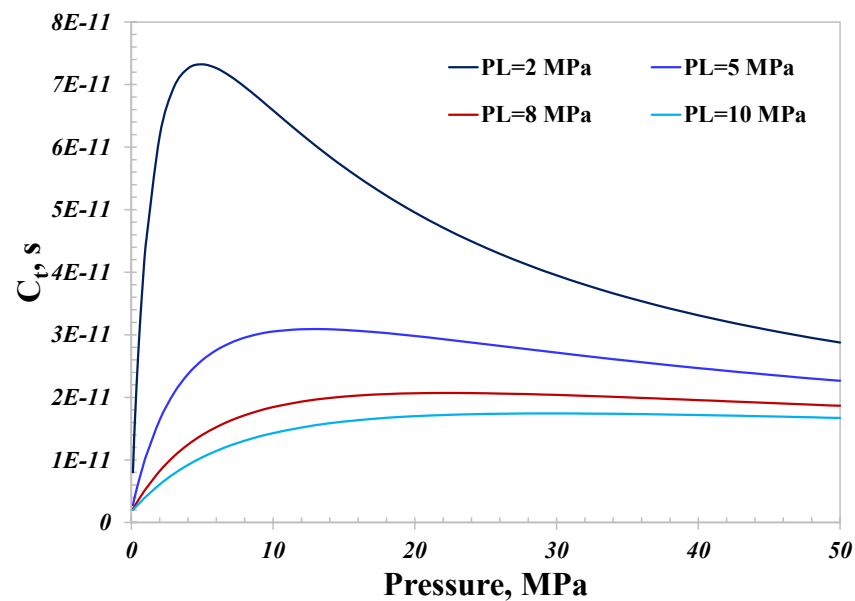


Figure 10. Total hydrogen flow conductance with different adsorption capacities.

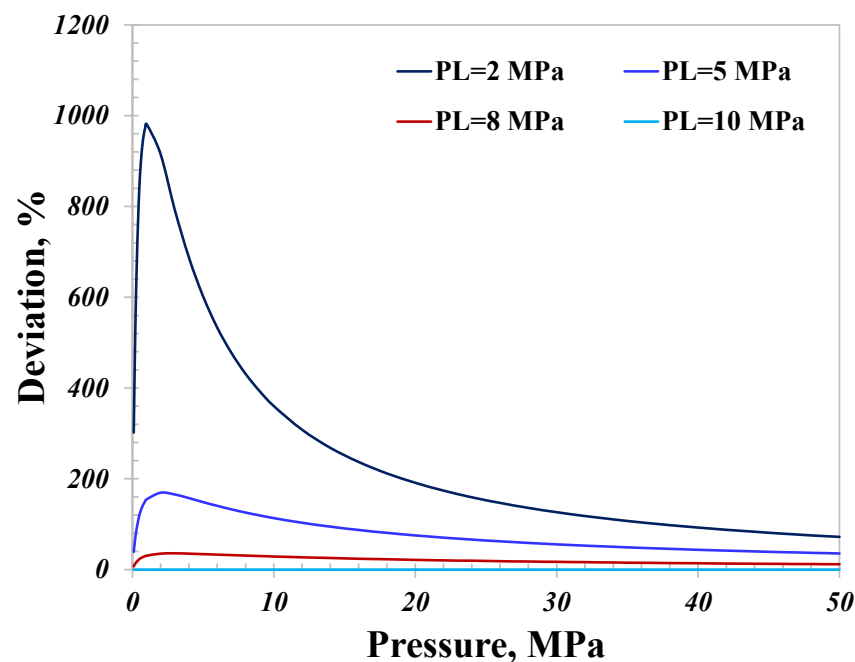


Figure 11. Deviation of the adsorption capacity by hydrogen flow conductance.

As for geological hydrogen storage, the main pore size of the specified storage site is crucial, determining the prominent transport mechanism. As for large nanopores (>30 nm), a low pressure and a high temperature are able to maintain a relatively low total conductance. In contrast, as for small nanopores (<10 nm), a high pressure and a low temperature could reduce the nanoconfined hydrogen flow capacity efficiently. A high pressure is able to reduce the hydrogen flow conductance as a result of a strong adsorption capacity.

Finally, it is necessary to clarify the research novelty accordingly. Although the model establishment framework including the bulk gas flow and surface diffusion is the same as that of the methane flow model for shale gas reservoirs, the presented hydrogen flow behavior in nanopores is completely different from the reported methane flow and the existing research on nanoconfined hydrogen flow. Notably, the main novelty of this research depends on the nanoconfined hydrogen flow behavior presented in the proposed model, rather than the proposed model itself, which elaborates the impacts of pressure, temperature and pore size on the hydrogen flow capacity in nanopores in detail. Compared with the methane flow in shale gas reservoirs, due to the great discrepancies in the physical attributes between hydrogen and methane, nanoconfined hydrogen flow physics could be dramatically different from methane flow physics. Apart from the bulk gas flow, hydrogen's adsorption capacity is much weaker than that of methane according to our recent research [44]; thus, it is necessary to explore the hydrogen flow in nanopores with a relatively weak adsorption capacity. Using the existing model for shale gas reservoirs fails to reveal the nanoconfined hydrogen flow behavior, which is mainly attributed to the different physical attributes of the gases, as well as their different adsorption capacities. Additionally, the majority of the current research describes nanoconfined hydrogen flow utilizing the Knudsen diffusion equation [8,9,45,46], inherently considering hydrogen flow physics in nanopores according to Knudsen diffusion, and the relevant Knudsen number is always greater than 10. The reliability of Knudsen diffusion for nanoconfined hydrogen flow holds under low-pressure conditions, as the mean free path calculated using Equation (3) becomes relatively large under low-pressure conditions, leading to the Knudsen number exceeding 10. However, in terms of geological hydrogen storage, hydrogen's pressure could reach as high as several tens of MPa, considerably reducing the mean free path and the Knudsen number. As a result, the Knudsen diffusion equation adopted by the existing research for hydrogen flow in nanopores may not characterize the hydrogen flow behavior during hydrogen geological storage over a wide pressure range. Therefore, the proposed model in this research, covering the entire Knudsen number range and all four types of gas flow physics, is a necessary and crucial supplement to the current research on nanoconfined hydrogen flow. In addition, the reported hydrogen flow behavior in the existing research is irrelevant given pressure and hydrogen's viscosity. In summary, the impact of pressure on nanoconfined hydrogen flow is a novel consideration, as is the studied hydrogen flow capacity in nanopores in this research.

5. Conclusions

- (1) A fundamental framework for nanoconfined hydrogen flow capacity is developed by coupling the bulk gas flow mechanism and the surface diffusion of adsorption hydrogen, accounting for the slip boundary and hydrogen's density and viscosity, as well as their variation over pressure and temperature. Two datasets of experimental results validate the proposed framework well with only a 6.3% difference on average. Also, the proposed model has an excellent match with the diffusion coefficients of Helium-3, which has a comparable kinetic diameter to hydrogen. In addition, more relevant underlying mechanisms could be further incorporated to improve the model accuracy.

- (2) The observation that the total conductance in small nanopores (<10 nm) may exceed that in large nanopores (>30 nm) is impressive, which conflicts with the conventional principle according to the classic Navier–Stokes equation. The prominent role surface diffusion has in small nanopores in affecting the nanoconfined hydrogen flow capacity is found to be responsible for this impressive observation. Also, the bulk gas flow would dominate the total conductance and the contribution of surface diffusion can be neglected in large nanopores.
- (3) The contribution of surface diffusion increases rapidly and then reduces stably with increasing pressure and is enhanced with an increasing temperature. The conductance contributed by the bulk gas flow almost linearly increases with increasing pressure and weakens with an increasing temperature. The adsorption capacity has a surprising influence on the total hydrogen conductance, particularly for small nanopores, and the conductance with strong adsorption ($P_L = 2$ MPa) could be 10 times as great as that with a weak adsorption capacity ($P_L = 10$ MPa).

Author Contributions: Methodology, Z.S.; Software, R.Q.; Formal analysis, Z.H.; Investigation, Y.W.; Visualization, W.L. All authors have read and agreed to the published version of the manuscript.

Funding: This work was supported by the National Natural Science Foundation of China (Grant No. 52204031) and the Natural Science Foundation of Sichuan Province (Grant No. 23NSFSC4527).

Data Availability Statement: Data are contained within the article.

Conflicts of Interest: The authors declare no conflicts of interest.

References

1. Habiba, U.M.M.E.; Xinbang, C.; Anwar, A. Do green technology innovations, financial development, and renewable energy use help to curb carbon emissions? *Renew. Energy* **2022**, *193*, 1082–1093. [[CrossRef](#)]
2. Godil, D.I.; Yu, Z.; Sharif, A.; Usman, R.; Khan, S.A.R. Investigate the role of technology innovation and renewable energy in reducing transport sector CO₂ emission in China: A path toward sustainable development. *Sustain. Dev.* **2021**, *29*, 694–707. [[CrossRef](#)]
3. Sun, Z.; Li, X.; Shi, J.; Zhang, T.; Sun, F. Apparent permeability model for real gas transport through shale gas reservoirs considering water distribution characteristic. *Int. J. Heat Mass Transf.* **2017**, *115*, 1008–1019. [[CrossRef](#)]
4. Yue, M.; Lambert, H.; Pahon, E.; Roche, R.; Jemei, S.; Hissel, D. Hydrogen energy systems: A critical review of technologies, applications, trends and challenges. *Renew. Sustain. Energy Rev.* **2021**, *146*, 111180. [[CrossRef](#)]
5. Aftab, A.; Hassanpouryouzband, A.; Xie, Q.; Machuca, L.L.; Sarmadivaleh, M. Toward a fundamental understanding of geological hydrogen storage. *Ind. Eng. Chem. Res.* **2022**, *61*, 3233–3253. [[CrossRef](#)]
6. Singh, H. Hydrogen storage in inactive horizontal shale gas wells: Techno-economic analysis for Haynesville shale. *Appl. Energy* **2022**, *313*, 118862. [[CrossRef](#)]
7. Yuan, L.; Stanley, A.; Dehghanpour, H.; Reed, A. Measurement of helium diffusion in Lotsberg Salt cores: A proxy to evaluate hydrogen diffusion. *Int. J. Hydrogen Energy* **2024**, *52*, 686–702. [[CrossRef](#)]
8. Zhang, L.; Wu, K.; Chen, Z.; Yu, X.; Li, J.; Yang, S.; Yang, M. Gas storage and transport in porous media: From shale gas to helium-3. *Planet. Space Sci.* **2021**, *204*, 105283. [[CrossRef](#)]
9. Frick, U.; Becker, R.H.; Pepin, R.O. Solar wind record in the lunar regolith Nitrogen and noble gases. In *Lunar and Planetary Science Conference Proceedings, Proceedings of the Lunar and Planetary Science Conference, Houston, TX, USA, 5–7 April 1988*; Lunar and Planetary Institute: Houston, TX, USA, 1988; pp. 87–120.
10. Romanenko, I.; Rajagopal, A.; Neumann, C.; Turchanin, A.; Streb, C.; Schacher, F.H. Embedding molecular photosensitizers and catalysts in nanoporous block copolymer membranes for visible-light driven hydrogen evolution. *J. Mater. Chem. A* **2020**, *8*, 6238–6244. [[CrossRef](#)]
11. Qin, Y.Q.; Gong, Y.; Yuan, Y.W.; Yang, Z.G. Failure analysis on leakage of hydrogen storage tank for vehicles occurring in oil circulation fatigue test. *Eng. Fail. Anal.* **2020**, *117*, 104830. [[CrossRef](#)]
12. Giri, A.; Hopkins, P.E. Heat transfer mechanisms and tunable thermal conductivity anisotropy in two-dimensional covalent organic frameworks with adsorbed gases. *Nano Lett.* **2021**, *21*, 6188–6193. [[CrossRef](#)] [[PubMed](#)]
13. Wang, H.; Chen, L.; Qu, Z.; Yin, Y.; Kang, Q.; Yu, B.; Tao, W.Q. Modeling of multi-scale transport phenomena in shale gas production—A critical review. *Appl. Energy* **2020**, *262*, 114575. [[CrossRef](#)]
14. Song, X.; Wang, L.A.; Gong, J.; Zhan, X.; Zeng, Y. Exploring a new method to study the effects of surface functional groups on adsorption of CO₂ and CH₄ on activated carbons. *Langmuir* **2020**, *36*, 3862–3870. [[CrossRef](#)] [[PubMed](#)]
15. Zhao, J.; Wang, J.; Zhang, G.; Zhou, D.; Chen, L.; Viswanathan, H.; Kang, Q. (Minireview on Lattice Boltzmann Modeling of Gas Flow and Adsorption in Shale Porous Media: Progress and Future Direction. *Energy Fuels* **2023**, *37*, 1511–1524. [[CrossRef](#)]

16. Chen, L.; He, A.; Zhao, J.; Kang, Q.; Li, Z.Y.; Carmeliet, J.; Tao, W.Q. Pore-scale modeling of complex transport phenomena in porous media. *Prog. Energy Combust. Sci.* **2022**, *88*, 100968. [[CrossRef](#)]
17. Liu, Z.; Emami-Meybodi, H. Apparent diffusion coefficient for adsorption-controlled gas transport in nanoporous media. *Chem. Eng. J.* **2022**, *450*, 138105. [[CrossRef](#)]
18. Zhang, H.; Wang, S.; Yin, X.; Qiao, R. Soaking in CO₂ huff-n-puff: A single-nanopore scale study. *Fuel* **2022**, *308*, 122026.
19. Sun, E.W.H.; Bourg, I.C. Molecular dynamics simulations of mineral surface wettability by water versus CO₂: Thin films, contact angles, and capillary pressure in a silica nanopore. *J. Phys. Chem. C* **2020**, *124*, 25382–25395. [[CrossRef](#)]
20. Beskok, A.; Karniadakis, G.E. Report: A model for flows in channels, pipes, and ducts at micro and nano scales. *Microscale Thermophys. Eng.* **1999**, *3*, 43–77.
21. Sun, Z.; Wu, K.; Shi, J.; Zhang, T.; Feng, D.; Wang, S.; Li, X. Effect of pore geometry on nanoconfined water transport behavior. *AIChE J.* **2019**, *65*, e16613. [[CrossRef](#)]
22. Wang, Z.; Jin, X.; Wang, X.; Sun, L.; Wang, M. Pore-scale geometry effects on gas permeability in shale. *J. Nat. Gas Sci. Eng.* **2016**, *34*, 948–957. [[CrossRef](#)]
23. Roy, S.; Raju, R.; Chuang, H.F.; Cruden, B.A.; Meyyappan, M. Modeling gas flow through microchannels and nanopores. *J. Appl. Phys.* **2003**, *93*, 4870–4879. [[CrossRef](#)]
24. Javadpour, F. Nanopores and apparent permeability of gas flow in mudrocks (shales and siltstone). *J. Can. Pet. Technol.* **2009**, *48*, 16–21. [[CrossRef](#)]
25. Shi, J.; Zhang, L.; Li, Y.; Yu, W.; He, X.; Liu, N.; Wang, T. Diffusion and flow mechanisms of shale gas through matrix pores and gas production forecasting. In Proceedings of the SPE Canada Unconventional Resources Conference, Calgary, AB, Canada, 5–7 November 2013; p. SPE-167226.
26. Wu, K.; Li, X.; Guo, C.; Wang, C.; Chen, Z. A unified model for gas transfer in nanopores of shale-gas reservoirs: Coupling pore diffusion and surface diffusion. *SPE J.* **2016**, *21*, 1583–1611. [[CrossRef](#)]
27. Gao, Y.; Wu, K.; Chen, Z.; Li, J.; Li, Q.; Dong, X.; Bi, J. Effect of surface force on nanoconfined shale-gas flow in slit channels. *SPE J.* **2021**, *26*, 448–460. [[CrossRef](#)]
28. Sun, Z.; Li, X.; Liu, W.; Zhang, T.; He, M.; Nasrabadi, H. Molecular dynamics of methane flow behavior through realistic organic nanopores under geologic shale condition: Pore size and kerogen types. *Chem. Eng. J.* **2020**, *398*, 124341. [[CrossRef](#)]
29. Cravero, C.; De Domenico, D.; Leutcha, P.J.; Marsano, D. Strategies for the numerical modelling of regenerative pre-heating systems for recycled glass raw material. *IETA Math. Model. Eng. Probl.* **2019**, *6*, 324–332. [[CrossRef](#)]
30. Chen, Y.; Li, Z.; Dai, Z.; Yang, F.; Wen, Y.; Shan, B.; Chen, R. Multiscale CFD modelling for conformal atomic layer deposition in high aspect ratio nanostructures. *Chem. Eng. J.* **2023**, *472*, 144944. [[CrossRef](#)]
31. Lynch, C.I.; Rao, S.; Sansom, M.S. Water in nanopores and biological channels: A molecular simulation perspective. *Chem. Rev.* **2020**, *120*, 10298–10335. [[CrossRef](#)]
32. Wen, C.; Zhang, S.L. Fundamentals and potentials of solid-state nanopores: A review. *J. Phys. D Appl. Phys.* **2020**, *54*, 023001. [[CrossRef](#)]
33. Asai, P.; Jin, J.; Deo, M.; Miller, J.D.; Butt, D. Non-equilibrium molecular dynamics simulation to evaluate the effect of confinement on fluid flow in silica nanopores. *Fuel* **2022**, *317*, 123373. [[CrossRef](#)]
34. Liu, L.; Wang, Y.; Aryana, S.A. Insights into scale translation of methane transport in nanopores. *J. Nat. Gas Sci. Eng.* **2021**, *96*, 104220. [[CrossRef](#)]
35. Zuo, H.; Zhai, C.; Deng, S.; Jiang, X.; Javadpour, F. Lattice Boltzmann modeling of gaseous microflow in shale nanoporous media. *Fuel* **2023**, *337*, 127087. [[CrossRef](#)]
36. Hatami, M.; Bayless, D.; Sarvestani, A. A model for stress-dependence of apparent permeability in nanopores of shale gas reservoirs. *AIChE J.* **2020**, *66*, e16541. [[CrossRef](#)]
37. Wu, S.; Fang, S.; Ji, L.; Wen, F.; Sun, Z.; Yan, S.; Li, Y. Transport Behavior of Methane Confined in Nanoscale Porous Media: Impact of Pore Evolution Characteristics. *Processes* **2022**, *10*, 2746. [[CrossRef](#)]
38. Wan, Y.; Niu, N.; Lu, W.; Zhou, Y.; Wang, B.; Lu, S. Unusual Water Flow in Ultra-Tight Porous Media: Integration of Profession and Innovation. *Processes* **2023**, *11*, 1245. [[CrossRef](#)]
39. Zhdanov, V.M.; Stepanenko, A.A. Separation of a Gas Mixture in Nanosize Porous Membranes. Effect of Adsorption and Surface Diffusion. *J. Eng. Phys. Thermophys.* **2021**, *94*, 623–632. [[CrossRef](#)]
40. Fanourgakis, G.S.; Gkagkas, K.; Tylanakis, E.; Froudakis, G. A generic machine learning algorithm for the prediction of gas adsorption in nanoporous materials. *J. Phys. Chem. C* **2020**, *124*, 7117–7126. [[CrossRef](#)]
41. Choma, J.; Jagiello, J.; Jaroniec, M. Assessing the contribution of micropores and mesopores from nitrogen adsorption on nanoporous carbons: Application to pore size analysis. *Carbon* **2021**, *183*, 150–157. [[CrossRef](#)]
42. Zamirian, M.; Aminian, K.; Ameri, S.; Fathi, E. New steady-state technique for measuring shale core plug permeability. In Proceedings of the SPE Canada Unconventional Resources Conference, Calgary, AB, Canada, 30 September–2 October 2014; p. D031S011R008.
43. Xia, L.; Zou, Z.J.; Wang, Z.H.; Zou, L.; Gao, H. Surrogate model based uncertainty quantification of CFD simulations of the viscous flow around a ship advancing in shallow water. *Ocean. Eng.* **2021**, *234*, 109206. [[CrossRef](#)]
44. Sun, Z.; Huang, B.; Wang, S.; Wu, K.; Li, H.; Wu, Y. Hydrogen adsorption in nanopores: Molecule-wall interaction mechanism. *Int. J. Hydrogen Energy* **2023**, *48*, 33496–33508. [[CrossRef](#)]

45. Frick, U.; Pepin, R.O. Microanalysis of nitrogen isotope abundances: Association of nitrogen with noble gas carriers in Allende. *Earth Planet Sci. Lett.* **1981**, *56*, 64–81. [[CrossRef](#)]
46. Nier, A.O.; Schlutter, D.J. Extraction of helium from individual IDPs and lunar grains by pulse heating. *Meteoritics* **1992**, *27*, 166–173. [[CrossRef](#)]

Disclaimer/Publisher’s Note: The statements, opinions and data contained in all publications are solely those of the individual author(s) and contributor(s) and not of MDPI and/or the editor(s). MDPI and/or the editor(s) disclaim responsibility for any injury to people or property resulting from any ideas, methods, instructions or products referred to in the content.